A FRAMEWORK FOR METAL FORMING SIMULATION

Rodrigo Rossi
Departamento de Engenharia Mecânica, Universidade de Caxias do Sul, Cidade Universitária, Bloco D, Caxias do Sul, RS, 95070-560, Brazil
rrossi@ucs.br

Marcelo Krajnc Alves
Departamento de Engenharia Mecânica, Universidade Federal de Santa Catarina, Campus Trindade, Florianópolis, SC, 88010-970, Brazil
krajnc@emc.ufsc.br

Abstract. *In this work the element-free Galerkin method is investigated when submitted to the large deformation process coupled with unilateral contact. The material model assumes the multiplicative decomposition of the deformation gradient into elastic and plastic parts and considers a J_2 elastoplastic constitutive relationship with a nonlinear isotropic hardening. The constitutive model is written in terms of the rotated Kirchoff stress and the logarithmic strain conjugate measure. A Total Lagrangian formulation is considered. The imposition of the essential boundary conditions is made by an augmented Lagrangian methodology. The contact formulation used in this work assumes the Signorini condition. To impose the contact the body is modeled using a triangular background integration mesh. Aspects related to the volumetric locking are also numerically investigated and a F-bar antivolumetric locking methodology type is proposed. Some numerical results are presented, under axisymmetric and plane strain assumption, in order to attest the performance of the proposed methodology.*

Keywords*: Finite strains, Mesh-free, EFG, Volumetric locking, Contact, Friction.*

1. Introduction

In this work it is presented a complete framework for metal forming simulation in the context element-free *Galerkin* method, EFG. More specifically, the proposed procedure considers a *Total Lagrangian* description; a multiplicative decomposition of the deformation gradient, into a plastic and an elastic part; a constitutive formulation, given in terms of the logarithmic deformation measure, ln(**U**), and the rotated *Kirchoff* stress. In this model the elastic response is assumed to be hyperelastic, according to the *Hencky* model, and the plastic model is given in terms of a J_2 plasticity model; a contact model based on the *Signorini* hypothesis together with a friction model that takes into account a regularized *Coulomb* law. The imposition of the essential boundary conditions is done by an augmented Lagrangian methodology.

Due to the incompressibility of the plastic flow a *F-bar* method is implemented, in the context of the mesh-free methods, and investigated under axisymmetric and plane strain conditions. Such choice is due to the simplicity of implementation of the method, when compared with the other methods, and due to the good results mention in the literature.

2. A brief description of the element-free galerkin method

Using the *Moving Least Square Approximation*, Lancaster and Salkuskas (1981), it is possible to construct an approximation function $u^h(\boldsymbol{X})$ that fits a discrete set of data $\{u_I, I=1\ldots n\}$ such that:

$$u^h(\boldsymbol{X}) = \sum_{I=1}^{n} \Phi_I(\boldsymbol{X}) u_I \,, \tag{1}$$

$$\Phi_I(\boldsymbol{X}) = \boldsymbol{p}(\boldsymbol{X}) \cdot \mathbf{A}(\boldsymbol{X})^{-1} \boldsymbol{b}_I(\boldsymbol{X}), \quad \mathbf{A}(\boldsymbol{X}) = \sum_{I=1}^{n} w(\boldsymbol{X} - \boldsymbol{X}_I)\left[\boldsymbol{p}(\boldsymbol{X}_I) \otimes \boldsymbol{p}(\boldsymbol{X}_I)\right] \quad \text{and} \quad \boldsymbol{b}_I(\boldsymbol{X}) = w(\boldsymbol{X} - \boldsymbol{X}_I)\boldsymbol{p}(\boldsymbol{X}_I) \tag{2}$$

where $\{p_j(\boldsymbol{X}), j=1\ldots m\}$ represents the set of intrinsic base functions and $w(\boldsymbol{X} - \boldsymbol{X}_I)$ is a weight function centered at $\boldsymbol{X}_I$. Here, $\Phi_I(\boldsymbol{X})$ is the global shape function, defined at particle $\boldsymbol{X}_I$, and $\mathbf{A}(\boldsymbol{X})$ is the moment matrix.

The conventional EFG method, Belytschko *et al.* (1994), can de described by the construction of a set of global shape functions, $\Phi_I(\boldsymbol{X})$ defined at particle $\boldsymbol{X}_I$. The particles distribution is not arbitrary since it must satisfy the following condition, Liu *et al.* (1997),

$$card\left\{\boldsymbol{X}_J \,\middle|\, \Phi_J(\boldsymbol{X}) \neq 0\right\} \geq \dim\left[\mathbf{A}(\boldsymbol{X})\right]. \tag{3}$$

In this work, $\boldsymbol{X} \in R^2$ with $\boldsymbol{X}=(X,Y)$, and the intrinsic base functions is $\boldsymbol{p}^T(\boldsymbol{X}) = [1,X,Y]$. Thus, from this condition, for all $\boldsymbol{X} \in \bar{\Omega}$, there must be at least three particles whose weight functions have a nonzero value at $\boldsymbol{X}$ and whose position vector forms a triangle with a non-zero area. In order to obtain a particle distribution that comply with Eq.(3), we perform a partition of the domain, Ω, into a triangular integration mesh. Many element-free Galerkin weight functions were proposal in the last years. In this work we use the quartic spline weight function given as:

$$w^{EFG}(r) = \begin{cases} 1 - 6r^2 + 8r^3 - 3r^4, & \text{for} \quad r \leq 1.0 \\ 0, & \text{for} \quad r > 1.0 \end{cases}. \tag{4}$$

Here, $r = r_I / \bar{r}_I$ with $r_I = \left\| \boldsymbol{X} - \boldsymbol{X}_I \right\|$. The radius $\bar{r}_I$, defining the support of $w^{EFG}(\boldsymbol{X} - \boldsymbol{X}_I)$, is determined by

$$\bar{r}_I = s \cdot r_{I\max}, \qquad s > 1, \;\; s \in R \;\text{ with }\; r_{I\max} = \max_i \left\| \boldsymbol{X}_i - \boldsymbol{X}_I \right\|, \quad i \in J_I \tag{5}$$

where J_I represents the set of adjacent nodes associated with $\boldsymbol{X}_I$.

Now, in the conventional EFG method, the global shape functions $\{\Phi_I(\boldsymbol{X}), I=1\ldots n\}$ do not satisfy, in general, the kronecker delta property, i.e., $\Phi_I(\boldsymbol{X}_J) \neq \delta_{IJ}$. As a consequence, it is not possible to enforce the essential boundary conditions, by directly prescribing nodal values, as done in the FEM.

3. Finite deformation description

The model considers the multiplicative decomposition of the **F** into an elastic and plastic parts, such that

$$\mathbf{F} = \mathbf{F}^e \mathbf{F}^p \tag{6}$$

with

$$\mathbf{F} = \nabla_X \boldsymbol{\varphi}(\boldsymbol{X}, t). \tag{7}$$

The consideration of a J_2 plasticity model leads to $\det(\mathbf{F}^p) = 1$ and, since $\det(\mathbf{F}) > 0$, implies that $\det(\mathbf{F}^e) > 0$. Thus, the elastic deformation gradient admits a polar decomposition, i.e.,

$$\mathbf{F}^e = \mathbf{R}^e \mathbf{U}^e \tag{8}$$

where $\mathbf{U}^e = \sqrt{\mathbf{C}^e}$ with $\mathbf{C}^e$ being the elastic right Cauchy-Green tensor given by $\mathbf{C}^e = \left(\mathbf{F}^e\right)^T \mathbf{F}^e$ and $\mathbf{R}^e$ being the elastic rotation tensor. The elastic deformation measure used in this work is the logarithmic or *Hencky* strain tensor given by

$$\mathbf{E}^e = \ln\left(\mathbf{U}^e\right). \tag{9}$$

The stress-strain pairs must be such that rate of work density remains preserved. Thus, the conjugate stress associated with the *Hencky* strain is the *rotated Kirchoff* stress $\bar{\boldsymbol{\tau}}$, given by

$$\bar{\boldsymbol{\tau}} = \left(\mathbf{R}^e\right)^T \boldsymbol{\tau} \mathbf{R}^e. \tag{10}$$

3.1. Constitutive formulation

The constitutive model investigated in this work considers a nonlinear isotropic hardening. In the frame work of the thermodynamic of irreversible process, the free energy potential is assumed to be of the form

$$\rho_o \psi\left(\mathbf{E}^e, \alpha\right) = \tfrac{1}{2}\mathbb{D}\mathbf{E}^e \cdot \mathbf{E}^e + \tfrac{1}{2} H \alpha^2 + \left(\sigma_\infty - \sigma_y\right)\left[\alpha + \tfrac{1}{\delta} e^{-\delta\alpha}\right]. \tag{11}$$

where ρ_o is the mass density, and H, δ, σ_∞ and σ_y are material parameters. $\mathbb{D}$ is the standard fourth order elastic constitutive relation. The state equations are given by

$$\bar{\boldsymbol{\tau}} = \rho_o \frac{\partial \psi}{\partial \mathbf{E}^e} = \mathbb{D}\mathbf{E}^e \tag{12}$$

for the rotated *Kirchoff* stress and

$$k = \rho_o \frac{\partial \psi}{\partial \alpha} = H\alpha + \left(\sigma_\infty - \sigma_y\right)\left(1 - e^{-\delta\alpha}\right) \tag{13}$$

for the isotropic hardening stress. Moreover, in this work we assume that

$$\bar{\mathbf{D}}^p = \dot{\lambda} \frac{\partial \mathcal{F}}{\partial \bar{\boldsymbol{\tau}}}, \tag{14}$$

and the hardening variable evolution is

$$\dot{\alpha} = -\dot{\lambda} \frac{\partial \mathcal{F}}{\partial k}. \tag{15}$$

The yield function used in this work assumes the following form,

$$\mathcal{F}\left(\bar{\boldsymbol{\tau}}, k\right) = \sqrt{3J_2} - \left[k\left(\alpha\right) + \sigma_y\right] \tag{16}$$

Here, $\dot{\lambda}$ is the plastic multiplier and must satisfy the following conditions

$$\mathcal{F} \leq 0 \qquad \dot{\lambda} \geq 0 \qquad \dot{\lambda}\mathcal{F} = 0. \tag{17}$$

4. Elasto-plastic initial value problem

The elasto-plastic problem presented in the previous section is dependent on the deformation history. Thus, in order to integrate the evolution equations from time step t_n to t_{n+1}, we must solve an initial value problem. The elasto-plastic initial value problem can be stated as, given the deformation history $\mathbf{F}(t), t \in [t_n, t_{n+1}]$ and

$$\mathbf{F}^p\left(t_n\right) = \mathbf{F}_n^p \;\; \textit{and} \;\; \alpha\left(t_n\right) = \alpha_n \tag{18}$$

determine $\mathbf{F}_{n+1}^p$ and α_{n+1} such that the Eq.(12), Eq.(14), Eq.(15) and Eq.(17) are satisfied. The strategy employed in the solution of the nonlinear problem comprises two basic steps that are: an elastic predictor and a plastic corrector.

- **Elastic predictor:** The solution is initially assumed as purely hyperelastic and a trial elastic state is computed by

$$\mathbf{F}_{n+1}^{e^{trial}} = \mathbf{F}_{n+1}\left(\mathbf{F}_n^p\right)^{-1} \quad \mathbf{C}_{n+1}^{e^{trial}} = \left(\mathbf{F}_{n+1}^{e^{trial}}\right)^T \mathbf{F}_{n+1}^{e^{trial}} \quad \mathbf{E}_{n+1}^{e^{trial}} = \frac{1}{2}\ln\left(\mathbf{C}_{n+1}^{e^{trial}}\right) \quad \bar{\boldsymbol{\tau}}_{n+1}^{trial} = \mathbb{D}\mathbf{E}_{n+1}^{e^{trial}} \quad \text{and} \quad k_{n+1}^{trial} = k_n \tag{19}$$

- **Plastic corrector:** The plastic corrector phase considers a *return mapping* algorithm that is obtained by the *backward exponential approximation* proposed in Eterovic & Bathe (1990) and Weber & Anand (1990). This phase consists in:
  - Verify the yield function feasibility: The plastic corrector is done only if $\mathcal{F}\left(\bar{\boldsymbol{\tau}}_{n+1}^{trial}, k_{n+1}^{trial}\right) > 0$.
  - Plastic correction: At this point the evolution laws are discretized. The plastic evolution $\dot{\mathbf{F}}^p = \bar{\mathbf{D}}^p\mathbf{F}^p$ is discretized based on the backward exponential approximation resulting in

$$\mathbf{F}_{n+1}^p = \exp\left(\bar{\mathbf{D}}_{n+1}^p\right)\mathbf{F}_n^p . \tag{20}$$

Moreover, after a straightforward manipulation, Eq.(20) reduces to

$$\mathbf{E}_{n+1}^e = \mathbf{E}_{n+1}^{e^{trial}} - \Delta\lambda\mathbf{N}_{n+1} \tag{21}$$

with

$$\mathbf{N}_{n+1} = \left.\frac{\partial\mathcal{F}}{\partial\bar{\boldsymbol{\tau}}}\right|_{n+1}, \quad \bar{\mathbf{D}}_{n+1}^p = \Delta\lambda\mathbf{N}_{n+1} \quad \text{and} \quad \mathbf{R}_{n+1}^e = \mathbf{R}_{n+1}^{e^{trial}} . \tag{22}$$

The discretized form of the remaining evolution equations is performed by a standard backward Euler method. Summarizing, the solution of plastic corrector phase is obtained by solving, for $\mathbf{E}_{n+1}^e$, α_{n+1} and $\Delta\lambda$,

$$\begin{cases} \mathbf{E}_{n+1}^e - \mathbf{E}_{n+1}^{e^{trial}} + \Delta\lambda\mathbf{N}_{n+1} \\ \alpha_{n+1} - \alpha_n - \Delta\lambda \\ \mathcal{F}\left(\bar{\boldsymbol{\tau}}_{n+1}, k\left(\alpha_{n+1}\right)\right) \end{cases} = \begin{bmatrix} 0 \\ 0 \\ 0 \end{bmatrix}. \tag{23}$$

5. Total lagrangean formulation

The problem can be enounced as: Determine ***u*** such that

$$\begin{aligned} \operatorname{div}\mathbf{P} - \rho_o\boldsymbol{b} &= \boldsymbol{0} \quad in\ \Omega_o \\ \mathbf{P}\boldsymbol{m} &= \boldsymbol{t} \quad in\ \Gamma_t \\ \boldsymbol{u} &= \bar{\boldsymbol{u}} \quad in\ \Gamma_u \end{aligned} \tag{24}$$

where $\mathbf{P}$ is the first Piola-Kirchoff stress, $\boldsymbol{b}$ is the body force vector, $\boldsymbol{m}$ is the outer normal on $\partial\Omega_o$, $\boldsymbol{t}$ is traction vector and $\bar{\boldsymbol{u}}$ is the prescribed displacement.

The called weak form of the Eq.(24), in the incremental form, can be posed as: Determine $\boldsymbol{u}_{n+1} \in H$ such that

$$\mathcal{G}\left(\boldsymbol{u}_{n+1}, \hat{\boldsymbol{u}}\right) = \int_{\Omega_o}\mathbf{P}\left(\boldsymbol{u}_{n+1}\right)\cdot\nabla_X\hat{\boldsymbol{u}}\ d\Omega_o - \int_{\Omega_o}\rho_o\boldsymbol{b}\cdot\hat{\boldsymbol{u}}\ d\Omega_o - \int_{\Gamma_{o_t}}\boldsymbol{t}\cdot\hat{\boldsymbol{u}}\ d\Gamma_{o_t} = 0 \quad \forall\,\hat{\boldsymbol{u}} \in H_o . \tag{25}$$

The solution of the nonlinear problem in Eq.(25) is achieved through a standard *Newton-Raphson* iteration method. In this context the linearization of the functional $\mathcal{G}\left(\boldsymbol{u}_{n+1}, \hat{\boldsymbol{u}}\right)$ is required. Assuming $\mathcal{G}$ to be sufficiently regular, we derive

$$\mathcal{G}\left(\boldsymbol{u}_{n+1}^k + \Delta\boldsymbol{u}_{n+1}^k, \hat{\boldsymbol{u}}\right) = \mathcal{G}\left(\boldsymbol{u}_{n+1}^k, \hat{\boldsymbol{u}}\right) + D\mathcal{G}\left(\boldsymbol{u}_{n+1}^k, \hat{\boldsymbol{u}}\right)\left[\Delta\boldsymbol{u}_{n+1}^k\right] \tag{26}$$

where

$$D\mathcal{G}\left(\boldsymbol{u}_{n+1}^k, \hat{\boldsymbol{u}}\right)\left[\Delta\boldsymbol{u}_{n+1}^k\right] = \int_{\Omega_o}\mathbb{A}\left(\boldsymbol{u}_{n+1}\right)\cdot\nabla_X\left(\Delta\boldsymbol{u}_{n+1}^k\right)\cdot\nabla_X\hat{\boldsymbol{u}}\ d\Omega_o \tag{27}$$

with

$$[\mathbb{A}]_{ijkl} = \frac{\partial P_{ij}}{\partial F_{kl}} = \frac{\partial\tau_{ip}}{\partial F_{kl}}F_{jp}^{-1} - \tau_{ip}F_{jk}^{-1}F_{lp}^{-1} . \tag{28}$$

By Eq.(28), the determination of $\mathbb{A}$ requires the derivative of the *Kirchoff* stress tensor with respect to the deformation gradient. As already seem, the *Kirchoff* stress is related to the rotated *Kirchoff* stress by Eq.(10). This means that in the determination of Eq.(28) a derivative of the rotated *Kirchoff* stress with respect to the deformation gradient takes place. But as $\bar{\boldsymbol{\tau}}_{n+1} = \hat{\bar{\boldsymbol{\tau}}}_{n+1}\left(\mathbf{E}_{n+1}^{e^{trial}}, (\bullet)_n\right)$ and by using the chain rule of differentiation, we derive

$$\hat{\mathbb{D}} = \frac{\partial\bar{\boldsymbol{\tau}}_{n+1}}{\partial\mathbf{F}_{n+1}} = \frac{\partial\bar{\boldsymbol{\tau}}_{n+1}}{\partial\mathbf{E}_{n+1}^{e^{trial}}}\frac{\partial\mathbf{E}_{n+1}^{e^{trial}}}{\partial\mathbf{C}_{n+1}^{e^{trial}}}\frac{\partial\mathbf{C}_{n+1}^{e^{trial}}}{\partial\mathbf{F}_{n+1}} = \tilde{\mathbb{D}}\mathbb{G}\mathbb{H} \tag{29}$$

The terms $\mathbb{G}$ and $\mathbb{H}$ in Eq.(29) are related with the geometric part of $\hat{\mathbb{D}}$ and are determined by

$$[\mathbb{H}]_{ijkl} = \frac{\partial C_{n+1_{ij}}^{e^{trial}}}{\partial F_{n+1_{kl}}} = F_{n_{li}}^{p^{-1}}F_{n+1_{kj}}^{e^{trial}} + F_{n+1_{ki}}^{e^{trial}}F_{n_{lj}}^{p^{-1}} \quad \text{and} \quad \mathbb{G} = \frac{\partial\mathbf{E}_{n+1}^{e^{trial}}}{\partial\mathbf{C}_{n+1}^{e^{trial}}} = \frac{\partial}{\partial\mathbf{C}_{n+1}^{e^{trial}}}\ln\left(\mathbf{U}_{n+1}^{e^{trial}}\right) = \frac{1}{2}\frac{\partial}{\partial\mathbf{C}_{n+1}^{e^{trial}}}\ln\left(\mathbf{C}_{n+1}^{e^{trial}}\right) \tag{30}$$

Notice that in the Eq.(30) a derivative of an isotropic tensor function is required, see details in Ortiz *et al.* (2001). Moreover, $\tilde{\mathbb{D}}$ is the only contribution related to the constitutive relation in the consistent tangent modulus $\mathbb{A}$. Its

determination depends if the state is elastic, $\mathcal{F} \le 0 \rightarrow \tilde{\mathbb{D}} = \mathbb{D}$, or elasto-plastic $\mathcal{F} > 0 \rightarrow \tilde{\mathbb{D}} = \mathbb{D}^{ep}$. Here, the elasto-plastic modulus is

$$\mathbb{D}^{ep} = \frac{d\overline{\boldsymbol{\tau}}_{n+1}}{d\mathbf{E}_{n+1}^{e^{trial}}} = \left(\mathbb{D}^{-1} + \Delta\lambda \frac{\partial \mathbf{N}_{n+1}}{\partial \overline{\mathbf{T}}_{n+1}} - \frac{1}{\frac{\partial \mathcal{F}}{\partial \alpha_{n+1}}} \mathbf{N}_{n+1} \otimes \mathbf{N}_{n+1} \right)^{-1} . \tag{31}$$

6. An F-Bar implementation

The *F-bar* methodology requires that the **F** be decomposed into a volumetric and an isochoric component

$$\mathbf{F} = \mathbf{F}_{iso}\mathbf{F}_{vol} \tag{32}$$

with $\mathbf{F}_{iso} = \det(\mathbf{F})^{\frac{1}{3}}\mathbf{F}$ and $\mathbf{F}_{vol} = \det(\mathbf{F})^{-\frac{1}{3}}\mathbf{I}$. Moreover, in the *F-bar* methodology the $\mathbf{F}_{vol}$ is computed as a constant inside the element. Thus, the *F-bar* is defined as

$$\overline{\mathbf{F}} = \mathbf{F}_{iso}\left(\mathbf{F}_a\right)_{vol} = \det(\mathbf{F})^{\frac{1}{3}} \det(\mathbf{F}_a)^{-\frac{1}{3}} \mathbf{F} . \tag{33}$$

Here we consider the average term $\det(\mathbf{F}_a)$ to be computed as

$$\det(\mathbf{F}_a) = \frac{1}{\Omega_e}\int_{\Omega_e} \det(\mathbf{F})\, d\Omega_e . \tag{34}$$

The derivation of the internal force in Eq.(25) and the tangent stiffness in Eq.(28) is achieved by making the following composition $\mathbf{P} = \mathbf{P} \circ \boldsymbol{\phi}(\mathbf{F})$ with $\boldsymbol{\phi}(\mathbf{F}) = \overline{\mathbf{F}}$. Thus,

$$[\overline{\mathbb{A}}]_{ijkl} = \frac{\partial P_{ij}}{\partial \overline{F}_{rs}} \frac{\partial \overline{F}_{rs}}{\partial F_{kl}} . \tag{35}$$

7. Contact and friction formulation

Figure 1 sketches the contact problem among a deformable body Ω and a rigid obstacle with frontier called Γ_{obs} which is parameterized by its arc length *l*. The role of frontier Γ_{obs} is to separate the space into an admissible region where the *gap function* $g < 0$, a contact region where $g = 0$ and into an inadmissible region where $g > 0$.

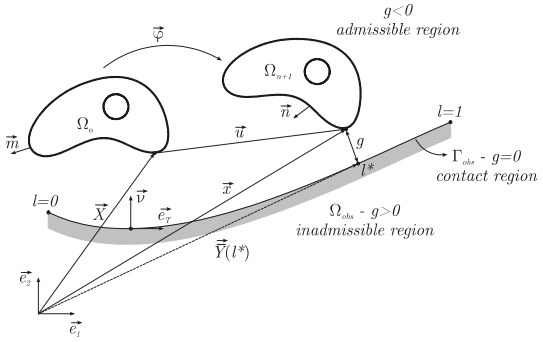

Figure 1 – Contact model problem in finite deformation.

In this context the *gap function* is given by

$$g(\boldsymbol{X},t) = -\boldsymbol{\nu}\cdot\left[\boldsymbol{x} - \overline{\boldsymbol{Y}}(l^*)\right] = -\boldsymbol{\nu}\cdot\left[\boldsymbol{X} + \boldsymbol{u} - \overline{\boldsymbol{Y}}(l^*)\right] \tag{36}$$

being l^* given by the solution of the following problem

$$l^* = \underset{l\in[0,1]}{\arg\min} \left\| \boldsymbol{X} + \boldsymbol{u} - \overline{\boldsymbol{Y}}(l) \right\| . \tag{37}$$

In a general manner the *Total Lagrangian* version of the *Signorini* contact problem can be written, in its incremental form, as: Determine $\boldsymbol{u}_{n+1} \in H$ such that

$$\tilde{\mathcal{G}}(\boldsymbol{u}_{n+1}, \hat{\boldsymbol{u}}) = \mathcal{G}(\boldsymbol{u}_{n+1}, \hat{\boldsymbol{u}}) + \mathcal{G}^u(\boldsymbol{u}_{n+1}, \hat{\boldsymbol{u}}) + \mathcal{G}^c(\boldsymbol{u}_{n+1}, \hat{\boldsymbol{u}}) = 0 \quad \forall\, \hat{\boldsymbol{u}} \in H_o \tag{38}$$

where

$$\mathcal{G}^u(\boldsymbol{u}_{n+1}, \hat{\boldsymbol{u}}) = -\int_{\Gamma_o^u} \boldsymbol{Q}_{n+1}^u \cdot \hat{\boldsymbol{u}}\; d\Gamma_o^u \quad \forall\, \hat{\boldsymbol{u}} \in H_o \;\text{ and }\; \mathcal{G}^c(\boldsymbol{u}_{n+1}, \hat{\boldsymbol{u}}) = -\int_{\Gamma_o^c} \boldsymbol{Q}_{n+1}^c \cdot \hat{\boldsymbol{u}}\; d\Gamma_o^c \quad \forall\, \hat{\boldsymbol{u}} \in H_o \tag{39}$$

being

$$\boldsymbol{Q}_{n+1}^u = \mathbf{P}_{n+1}\boldsymbol{m} \;\text{ on } \Gamma_o^u \quad \text{and} \quad \boldsymbol{Q}_{n+1}^c = Q_{\nu_{n+1}}^c \boldsymbol{\nu} + Q_{T_{n+1}}^c \boldsymbol{e}_T \;\text{ on } \Gamma_o^c \tag{40}$$

The scalar Q_ν^c is the term due to the normal contact and is given by $Q_{\nu_{n+1}}^c = \mathbf{P}_{n+1}\boldsymbol{m}\cdot\boldsymbol{\nu}$ and the scalar Q_T^c is the term due to the contribution tangential force which depends on the friction law adopted.

7.1. Imposition of the essential boundary conditions

In this work is proposed that the imposition of the essential boundary conditions being made by the *augmented Lagrangian* method. In this context the term $\boldsymbol{Q}^{u}_{n+1}$ can be expressed as

$$\boldsymbol{Q}^{u}_{n+1} = -\left[\boldsymbol{\lambda}_{u_{n+1}} + \epsilon_u \left(\boldsymbol{u}_{n+1} - \overline{\boldsymbol{u}}\right)\right] \quad \text{on } \Gamma^u_o \tag{41}$$

where $\boldsymbol{\lambda}^{h}_{u_{n+1}}$ and ϵ_u are the *Lagrange* multiplier and the penalty parameter associated with the imposition of the essential boundary conditions. Now, by using the EFG approximation $\boldsymbol{u}^{h}_{n+1}$ as commented in a earlier section one can rewrite the local Eq.(1) into its global form as

$$\boldsymbol{u}^{h}_{n+1} = \boldsymbol{\Phi}^{g}\boldsymbol{u}^{g}_{n+1}, \tag{42}$$

where $\boldsymbol{\Phi}^{g}$ is the global EFG shape function matrix and $\boldsymbol{u}^{g}_{n+1}$ is the global vector of unknowns. Through a similar manner let us admit a linear approximation to construct $\boldsymbol{\lambda}^{h}_{u_{n+1}}$

$$\boldsymbol{\lambda}^{h}_{u_{n+1}} = \mathbf{N}^{g}\boldsymbol{\lambda}^{g}_{u_{n+1}} \tag{43}$$

where $\mathbf{N}^{g}$ is the global linear shape function matrix. Substituting Eq.(43), Eq.(42) into Eq.(41) and this last into Eq.(39) one can derive

$$\mathcal{G}^{u}\left(\boldsymbol{u}^{h}_{n+1}, \hat{\boldsymbol{u}}^{h}\right) = -\int_{\Gamma^u_o} \boldsymbol{Q}^{u}_{n+1}\cdot\hat{\boldsymbol{u}}^{h}\, d\Gamma^u_o \quad \forall\, \hat{\boldsymbol{u}}^{h} \in H^{h} = \boldsymbol{f}^{\lambda_u}_{n+1}\cdot\hat{\boldsymbol{u}}^{g} + \boldsymbol{f}^{u}_{n+1}\cdot\hat{\boldsymbol{u}}^{g} \tag{44}$$

with

$$\boldsymbol{f}^{\lambda_u}_{n+1} = -\int_{\Gamma^u_o}\left(\boldsymbol{\Phi}^{g}\right)^{T}\mathbf{N}^{g}\boldsymbol{\lambda}^{g}_{u_{n+1}}\, d\Gamma^u_o \quad \text{and} \quad \boldsymbol{f}^{u}_{n+1} = -\epsilon_u\int_{\Gamma^u_o}\left(\boldsymbol{\Phi}^{g}\right)^{T}\boldsymbol{\Phi}^{g}\left(\boldsymbol{u}^{g}_{n+1} - \overline{\boldsymbol{u}}^{g}\right) d\Gamma^u_o\,. \tag{45}$$

The linearization of the Eq.(44) leads to

$$\mathcal{D}\mathcal{G}^{u}\left(\boldsymbol{u}_{n+1}, \hat{\boldsymbol{u}}\right)\left[\Delta\boldsymbol{u}_{n+1}\right] = -\epsilon_u\int_{\Gamma^u_o}\Delta\boldsymbol{u}_{n+1}\cdot\hat{\boldsymbol{u}}\; d\Gamma^u_o \tag{46}$$

and using the approximation

$$\mathcal{D}\mathcal{G}^{u}\left(\boldsymbol{u}^{h}_{n+1}, \hat{\boldsymbol{u}}^{h}\right)\left[\Delta\boldsymbol{u}^{h}_{n+1}\right] = \mathbf{K}^{u}_{n+1}\Delta\boldsymbol{u}^{g}_{n+1}\cdot\hat{\boldsymbol{u}}^{g} \quad \therefore \quad \mathbf{K}^{u}_{n+1} = -\epsilon_u\int_{\Gamma^u_o}\left(\boldsymbol{\Phi}^{g}\right)^{T}\boldsymbol{\Phi}^{g}\, d\Gamma^u_o\,. \tag{47}$$

7.2. Contact and friction terms

The function $\mathcal{G}^{c}$ is decomposed in the following form,

$$\mathcal{G}^{c}\left(\boldsymbol{u}_{n+1}, \hat{\boldsymbol{u}}\right) = \mathcal{G}^{c}_{\nu}\left(\boldsymbol{u}_{n+1}, \hat{\boldsymbol{u}}\right) + \mathcal{G}^{c}_{T}\left(\boldsymbol{u}_{n+1}, \hat{\boldsymbol{u}}\right), \tag{48}$$

with

$$\mathcal{G}^{c}_{\nu}\left(\boldsymbol{u}_{n+1}, \hat{\boldsymbol{u}}\right) = -\int_{\Gamma^c_o} Q^{c}_{\nu_{n+1}}\boldsymbol{\nu}\cdot\hat{\boldsymbol{u}}\, d\Gamma^c_o \quad \text{and} \quad \mathcal{G}^{c}_{T}\left(\boldsymbol{u}_{n+1}, \hat{\boldsymbol{u}}\right) = -\int_{\Gamma^c_o} Q^{c}_{T_{n+1}}\boldsymbol{e}_T\cdot\hat{\boldsymbol{u}}\, d\Gamma^c_o\,. \tag{49}$$

7.2.1. Imposition of the normal contact

Following the *augmented Lagrangian* procedure presented by Simo & Laursen (1992) this term is such that

$$Q^{c}_{\nu_{n+1}} = \left\langle \lambda_{N_{n+1}} + \epsilon_N g\left(\boldsymbol{u}_{n+1}\right)\right\rangle \quad \text{on } \Gamma^c_o \tag{50}$$

where λ_N and ϵ_N are, respectively, the *Lagrange* multiplier and the penalty parameter associated with the imposition of the normal contact and $\langle\bullet\rangle$ is the Macauley bracket. By introducing the approximations into Eq.(50) and substituting this in Eq.(49) one can derive

$$\mathcal{G}^{c}_{\nu}\left(\boldsymbol{u}^{h}_{n+1}, \hat{\boldsymbol{u}}^{h}\right) = -\int_{\Gamma^c_o} Q^{c}_{\nu_{n+1}}\boldsymbol{\nu}\cdot\hat{\boldsymbol{u}}^{h}\, d\Gamma^c_o = \boldsymbol{f}^{c}_{\nu_{n+1}}\cdot\hat{\boldsymbol{u}}^{g} \quad \therefore \quad \boldsymbol{f}^{c}_{\nu_{n+1}} = -\int_{\Gamma^c_o} Q^{c}_{\nu_{n+1}}\left(\boldsymbol{\Phi}^{g}\right)^{T}\boldsymbol{\nu}\; d\Gamma^c_o\,. \tag{51}$$

And its linearization leads to

$$\mathcal{D}\mathcal{G}^{c}_{\nu}\left(\boldsymbol{u}^{h}_{n+1}, \hat{\boldsymbol{u}}^{h}\right)\left[\Delta\boldsymbol{u}^{h}_{n+1}\right] = \mathbf{K}^{c}_{\nu_{n+1}}\Delta\boldsymbol{u}^{g}_{n+1}\cdot\hat{\boldsymbol{u}}^{g} \quad \therefore \quad \mathbf{K}^{c}_{\nu_{n+1}} = \epsilon_N\int_{\Gamma^c_o} H\left(Q^{c}_{\nu_{n+1}}\right)\left[\left(\boldsymbol{\Phi}^{g}\right)^{T}\boldsymbol{\nu}\right]\otimes\left[\left(\boldsymbol{\Phi}^{g}\right)^{T}\boldsymbol{\nu}\right] d\Gamma^c_o \tag{52}$$

7.2.2. Imposition of the tangential contact – friction

The complete determination of the tangential term, friction term, depends on the friction law adopted. In this work a regularized *Coulomb* friction law is used. This law can be derived by the introducing a penalty parameter into the classical *Coulomb* evolution friction law, for more complete discussion see Laursen (2002). In this framework the imposition of the friction law implies in the fulfillment of the following set of equations:

$$\begin{aligned} &\Upsilon\left(Q^{c}_{\nu_{n+1}}, Q^{c}_{T_{n+1}}\right) = \left|Q^{c}_{T_{n+1}}\right| - f_c Q^{c}_{\nu_{n+1}} \\ &\dot{Q}^{c}_{T_{n+1}} = -\epsilon_T\left(\dot{u}_{T_{n+1}} + \dot{\gamma}Q^{c}_{T_{n+1}}\left|Q^{c}_{T_{n+1}}\right|^{-1}\right) \text{ with } \dot{\gamma}\geq 0 \quad \text{and} \quad \dot{\gamma}\Upsilon = 0 \end{aligned} \tag{53}$$

where Υ is the called slip function, which plays the role of the yield function in the plasticity theory, f_c is the friction coefficient and $\dot{u}_T$ is the tangential velocity given, in the two-dimensional case, by $\dot{u}_T = \dot{\boldsymbol{u}} \cdot \boldsymbol{e}_T$.

The slip function take into account two conditions, the called stick condition for $\Upsilon \leq 0$ and the slip condition for $\Upsilon > 0$. Similarly as in the elastoplastic theory here is also assumed a trial procedure followed by a return mapping procedure. In this context the following algorithm is applicable:

Given $Q^c_{T_n}, Q^c_{\nu_{n+1}}, u^h_{T_{n+1}}$ and $u^h_{T_n}$, compute

$$Q^{c^{trial}}_{T_{n+1}} = Q^c_{T_n} - \epsilon_T \left(u^h_{T_{n+1}} - u^h_{T_n} \right) \tag{54}$$

Check the trial state

If $\Upsilon\left(Q^c_{\nu_{n+1}}, Q^{c^{trial}}_{T_{n+1}}\right) \leq 0$ then

stick condition: $Q^c_{T_{n+1}} = Q^{c^{trial}}_{T_{n+1}}$

Otherwise

slip condition: $Q^c_{T_{n+1}} = f_c Q^{c^{trial}}_{\nu_{n+1}} Q^{c^{trial}}_{T_{n+1}} \left| Q^{c^{trial}}_{T_{n+1}} \right|^{-1}$

end

Now, it is possible announce the approximate work done by the tangential forces as

$$\mathcal{G}^c_T\left(\boldsymbol{u}^h_{n+1}, \hat{\boldsymbol{u}}^h\right) = -\int_{\Gamma^c_o} Q^c_{T_{n+1}} \boldsymbol{e}_T \cdot \hat{\boldsymbol{u}}^h \, d\Gamma^c_o = \boldsymbol{f}^c_{T_{n+1}} \cdot \hat{\boldsymbol{u}}^g \quad \therefore \quad \boldsymbol{f}^c_{T_{n+1}} = -\int_{\Gamma^c_o} Q^c_{T_{n+1}} \left(\boldsymbol{\Phi}^g\right)^T \boldsymbol{e}_T \, d\Gamma^c_o \,. \tag{55}$$

With regard to the algorithm, the linearization of the Eq.(55) must take into account the stick-slip condition. Thus:

Stick linearization:

$$\mathcal{D}\mathcal{G}^c_T\left(\boldsymbol{u}^h_{n+1}, \hat{\boldsymbol{u}}^h\right)\left[\Delta \boldsymbol{u}^h_{n+1}\right] = \mathbf{K}^{c^{Stick}}_{T_{n+1}} \Delta \boldsymbol{u}^g_{n+1} \cdot \hat{\boldsymbol{u}}^g \qquad \therefore \qquad \mathbf{K}^{c^{Stick}}_{T_{n+1}} = \epsilon_T \int_{\Gamma^c_o} \left[\left(\boldsymbol{\Phi}^g\right)^T \boldsymbol{e}_T\right] \otimes \left[\left(\boldsymbol{\Phi}^g\right)^T \boldsymbol{e}_T\right] d\Gamma^c_o \tag{56}$$

Slip linearization:

$$\mathcal{D}\mathcal{G}^c_T\left(\boldsymbol{u}^h_{n+1}, \hat{\boldsymbol{u}}^h\right)\left[\Delta \boldsymbol{u}^h_{n+1}\right] = \mathbf{K}^{c^{Slip}}_{T_{n+1}} \Delta \boldsymbol{u}^g_{n+1} \cdot \hat{\boldsymbol{u}}^g \quad \therefore \quad \mathbf{K}^{c^{Slip}}_{T_{n+1}} = \epsilon_N f_c \int_{\Gamma^c_o} H\left(Q^c_{\nu_{n+1}}\right) \operatorname{sign}\left(Q^{c^{Trial}}_{T_{n+1}}\right) \left[\left(\boldsymbol{\Phi}^g\right)^T \boldsymbol{\nu}\right] \otimes \left[\left(\boldsymbol{\Phi}^g\right)^T \boldsymbol{e}_T\right] d\Gamma^c_o \tag{57}$$

7.3. Global algorithm

1. Given the load step for t_{n+1}, initialize $k = 0$ and ϵ_N, ϵ_T e ϵ_u with proper values, see examples section;
2. Initialize the multipliers and the global displacement vector with the values converged in the last iteration: $\lambda^{g^k}_{N_{n+1}} = \lambda^{g^k}_{N_n}$, $\boldsymbol{\lambda}^{g^k}_{u_{n+1}} = \boldsymbol{\lambda}^{g^k}_{u_n}$ and $\boldsymbol{u}^g_{n+1} = \boldsymbol{u}^g_{n+1}$;
3. Do while $\left(\left\| \boldsymbol{u}^{h^k}_{n+1} - \overline{\boldsymbol{u}}^h_{n+1} \right\|_\infty > tol_1 \text{ or } \left\| \left\langle g\left(\boldsymbol{u}^{h^k}_{n+1}\right) \right\rangle \right\|_\infty > tol_2 \right)$

   Obtain the solution $\boldsymbol{u}^{h^k}_{n+1}$ considering: $\tilde{\mathcal{G}}\left(\boldsymbol{u}^{h^k}_{n+1}, \hat{\boldsymbol{u}}^h\right) = \mathcal{G}\left(\boldsymbol{u}^{h^k}_{n+1}, \hat{\boldsymbol{u}}^h\right) + \mathcal{G}^u\left(\boldsymbol{u}^{h^k}_{n+1}, \hat{\boldsymbol{u}}^h\right) + \mathcal{G}^c\left(\boldsymbol{u}^{h^k}_{n+1}, \hat{\boldsymbol{u}}^h\right) = 0 \quad \forall \hat{\boldsymbol{u}}^h \in H^h$

   Once $\boldsymbol{u}^{h^k}_{n+1}$ has been converged it is necessary perform the following updates:

   Lagrange multipliers: $\boldsymbol{\lambda}^{g^{k+1}}_{u_{n+1}} = -\left[\boldsymbol{\lambda}^{g^k}_{u_{n+1}} + \epsilon_u \left(\boldsymbol{u}^{h^k}_{n+1} - \overline{\boldsymbol{u}}^h_{n+1}\right)\right] \qquad \lambda^{g^{k+1}}_{N_{n+1}} = \left\langle \lambda^{g^k}_{N_{n+1}} + \epsilon_N g\left(\boldsymbol{u}^{h^k}_{n+1}\right) \right\rangle$;

   Global displacement vector: $\boldsymbol{u}^{g^{k+1}}_{n+1} = \boldsymbol{u}^{g^k}_{n+1}$;

   Iteration k: $k \leftarrow k+1$;

   Once the conditions established in step 3 are satisfied is necessary to proceed with the update of not only the elastoplastic internal variables of the problem but also the variables associated with contact problem

   $\boldsymbol{Q}^u_{n+1} \leftarrow \boldsymbol{Q}^{u^k}_{n+1} \quad Q^c_{T_{n+1}} \leftarrow Q^{c^k}_{T_{n+1}} \quad Q^c_{\nu_{n+1}} \leftarrow Q^{c^k}_{\nu_{n+1}} \quad \boldsymbol{Q}^c_{\nu_{n+1}} \leftarrow Q^c_{\nu_{n+1}} \boldsymbol{\nu} + Q^c_{T_{n+1}} \boldsymbol{e}_T \quad u^h_{T_{n+1}} \leftarrow u^{h^k}_{T_{n+1}}$;
4. Perform the pos-processing operations;
5. Update the *n-th* iteration: $n \leftarrow n+1$
6. Proceeds to the new load increment and goes to step 1.

8. Examples

8.1. Upsetting of a cylinder

In this example is presented the upsetting of a cylinder with dimensions shown in Figure 2(a). Due to the symmetry of the problem only a quarter of the model is modeled with an integration mesh contends 12×16 triangular cells and 221 EFG particles, see Figures 2(b) and (c) respectively.

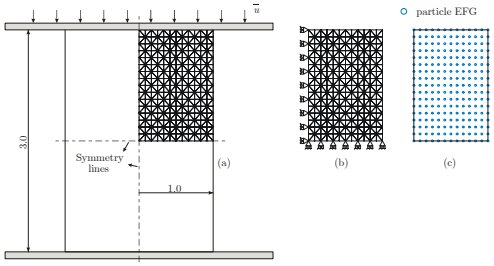

Figure 2 – Upsetting of a cylinder model.

The analysis consists of the movement of the superior wall, upsetting, of u_z = 1.2 *mm* with regard to horizontal symmetry line. The data used in this analysis are: κ = 164206.35 MPa, μ = 80193.80 MPa, H = 129.24 MPa, δ = 16.93, σ_∞ = 715 MPa, σ_y = 450 MPa, f_c = 0.2, ϵ_N =10^6, ϵ_T =10^4, ϵ_u =10^9, tol_1 = 10^{-5} and tol_2 = 10^{-6}.

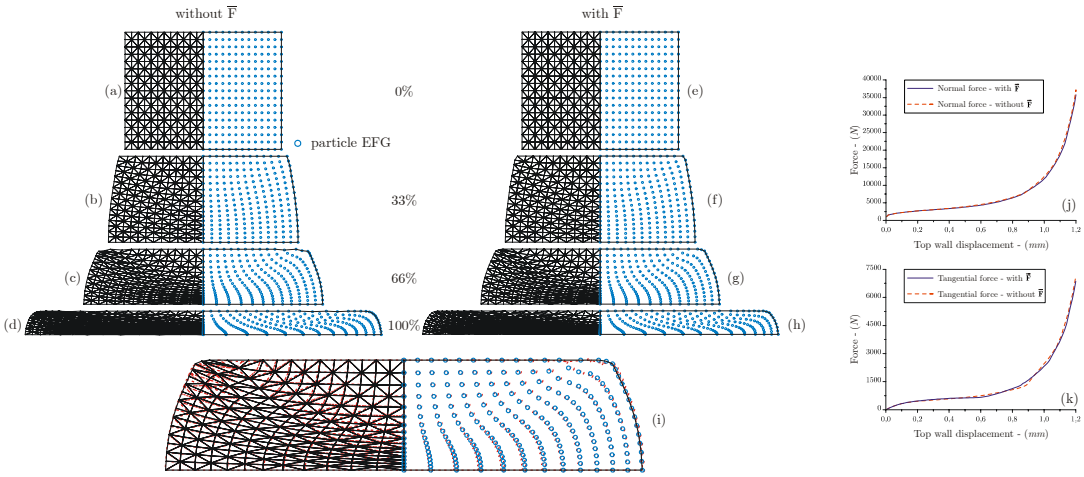

Figure 3 – Deformed results. (a) to (d) deformed configurations without *F-bar*; (e) to (f) deformed configurations with *F-bar*; (i) superposition of the results (c) and (g), (j) and (k) are the contact forces.

The results of this simulation, deformed configurations, are shown in Figure 3 considering an analysis with and without the presented anti-volumetric locking methodology. More specifically, Figure 3(a)-(d) presents the analysis without *F-bar* and Figure 3(e)-(f) presents the same analysis, however using the methodology *F-bar*. In Figure 3(i) it is presented the superposition of the deformed configuration, in a magnified scale, of the cases 3(c), represented in red color lines for better visualization, and 3(g). Notice that a sensible difference exists among the two deformed configurations, mainly in the contact corners region. The developed total forces during the process, in the contact superior wall, are shown in Figure 3(i) and (j), also considering the simulation with and without *F-bar*. Notice that in this case the differences are rather insignificant. However in both the cases the prediction of the total force was slightly inferior for the simulations using the *F-bar* strategy.

8.2. Cold forging of a mechanical component

In this example the simulation of a cold forging of a mechanical component is presented. The dimensions of the preform as well as the dimensions of the mold are shown in Figure 4. The process consists of the movement of the superior part of the mold of u_z = 60 *mm* in some steps to conform the preform into the mold. Due the symmetry, only a half of the component is modeled under axisymmetric hypothesis. In Figure 5(a) it is shown the initial integration mesh, together with its corresponding particle distribution. In this example 486 EFG particles into a integration mesh of 880 triangular cells had been used. The results are shown in the sequence of Figures 5(a)-(f) correspond the analysis without *F-bar*, and in Figure 5(g)-(l) are the output taken into consideration the *F-bar*. Figure 5(m) corresponds to the superposition of Figure 5(f) and 5(l). To make possible the visualization and interpretation the deformed configuration without the *F-bar* effect is shown in dashed lines in this last figure. Figure 5(n) depicts the evolution of the forging force necessary to conform the mechanical component. The total forces at the end of the process are F_z = 218753.45 *kN* for the problem considering *F-bar* and F_z = 215532.71 *kN* for the simulation without *F-bar*. The material parameters used in this example are the same used in the last example.

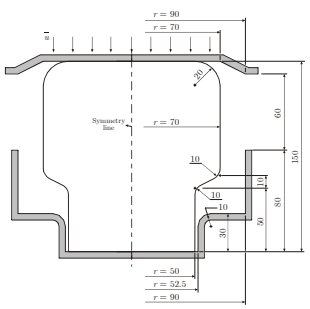

Figure 4 – Upsetting of a component model.

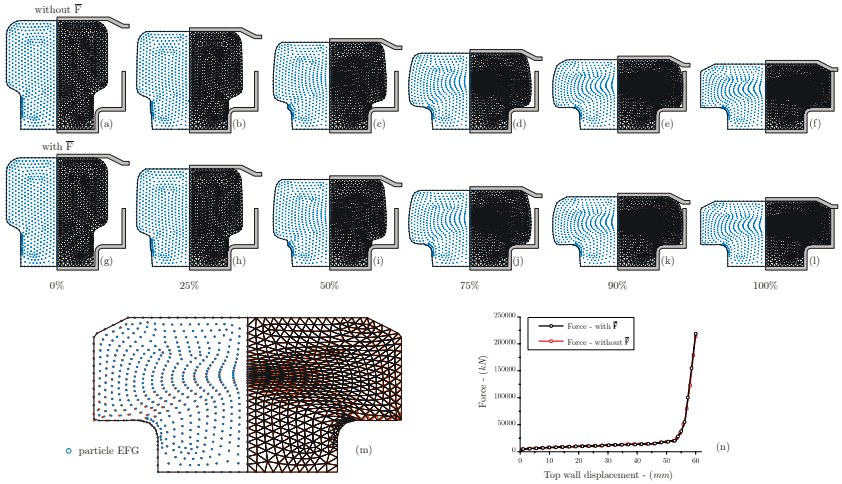

Figure 5 – (a)-(m) Deformed results – (n) forging forces.

Figure 6 presents the results for the accumulated plastic strain at the end of the analysis. Notice that, although small, a difference between the analysis with and without the anti-volumetric locking procedure exists. This difference is also noticed when the results for the von Mises equivalent stress are compared at the end of the analysis, Figure 7.

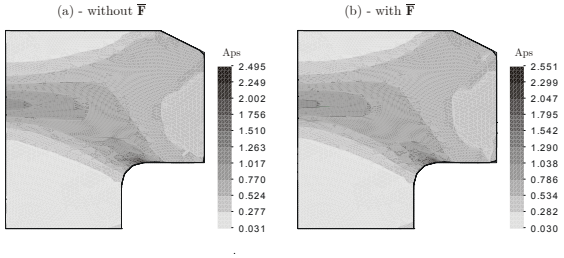

Figure 6 – Accumulated plastic strain output.

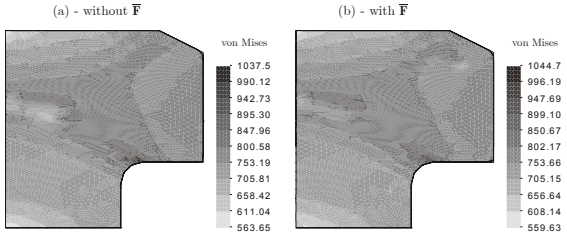

Figure 7 – von Mises equivalent stress output.

7. Conclusion

In this work the element-free *Galerkin* method was numerically investigated under unilateral contact in finite strains. Results shown in this paper evidence the presence of volumetric locking. Also it shows an improvement of the results since the *F-bar* approach is employed. The main large deformation-contact algorithm presented in this paper is robust and stable, providing good convergence rates.

8. References

Belytschko, T., Lu, Y.Y., Gu, L. (1994), Element-free Galerkin methods, *International Journal for Numerical Methods in Engineering*, vol. 37, pp. 229-256.

Lancaster, P., Salkuskas, K. (1981), "Surfaces generated by moving least square methods", *Mathematical of Computational*, vol. 37, pp. 141-158.

Laursen, T.A. (2002), Computational contact and impact mechanics, Springer, Germany, pp. xv + 454.

Liu, W.K., Li, S., Belytschko T. (1997), "Moving least-square reproducing kernel methods (I) Methodology and convergence", *Computer Methods in Applied Mechanics and Engineering*, vol. 147, pp. 113-154.

Ortiz M., Radovitzky, R.A., Repeto, E.A. (2001), "The computation of exponential and logarithmic mappings and their fisrt and second linearizations", *International Journal for Numerical Methods in Engineering*, vol. 52, pp. 1431-1441.

Simo, J.C., Armero, F. (1992), "Geometrically Non-Linear Enhanced Strain Mixed Methods and the Method of Incompatible Modes", *International Journal for Numerical Methods in Engineering*, vol. 33, pp. 1413-1449.

Simo, J.C., Laursen, T.A. (1992), "An augmented Lagrangian treatment of contact problems involving friction", *Computers & Structures*, vol. 42, pp. 97-116.

Souza Neto, E.A., Peric, D., Dutko, M., Owen, D.R.J. (1996), "Design of simple low order finite elements for large strain analysis of nearly incompressible solids", *International Journal of Solids and Structures*, vol. 33, pp. 3277-3296.

9. Acknowledgements

The support of the CNPq, Conselho Nacional de Desenvolvimento Científico e Tecnológico, of Brazil is gratefully acknowledged. Grant Numbers: 141806/2000-1 and 304020/2003-6.

10. Responsibility notice

The authors are the only responsible for the printed material included in this paper.